

The Effect of Joint Elasticity on Bilateral Teleoperation

M. Tavakoli and R.D. Howe

School of Engineering and Applied Sciences, Harvard University, Cambridge, MA 02138, USA
 {tavakoli, howe} @ seas.harvard.edu

Abstract—In applications such as space and surgical robotics, the use of thin, lightweight manipulators and cable-driven end-effectors results in flexibility of the manipulator. In bilateral teleoperation, however, any flexibility in a link or joint of the robot reduces the transparency of teleoperation. In this paper, we analyze master-slave teleoperation transparency under slave robot joint elasticity and evaluate the added benefits of using extra sensors at the end-effector of the elastic-joint robot. It is shown that velocity (or position) feedback from the output shaft of the elastic joint improves free-space position tracking performance, which in the absence of such feedback is hampered by the joint's anti-resonance. Also, when the interaction forces with an environment are measured by a force sensor and fed back to the user, end-effector velocity feedback improves hard-contact force tracking performance. If the operating trajectories correspond to low frequencies, both free-space position tracking and hard-contact force tracking are satisfactory regardless of end-effector feedback, yet the elasticity in the joint will be transmitted to the user during a hard contact task unless end-effector velocity feedback is used.

I. Introduction

In certain applications including space and surgical robotics, the desire is to use thin and lightweight manipulators and cable-driven end-effectors. Space robots are designed to be lightweight and compact for minimum liftoff cost and energy consumption during robot control, and therefore involve flexibility. Also, in robot-assisted port-access surgery, thin instruments (< 3 mm in pediatric surgery) are used for minimal invasiveness, which brings about advantages such as reduced trauma to the body, post-operative pain and length of hospital stay. Due to the limited space and the small diameter of the instruments, actuation of a distal wrist that is used for dexterity is performed from outside the patient and propagated to the wrist through flexible cables. Therefore, in addition to link flexibility, joint flexibility is present in such robots.

In the presence of joint or link flexibility, control laws based on the assumption of a rigid robot may no longer be effective or accurate due to the alteration of the kinematic and dynamic characteristics of the manipulator. An example application in which joint flexibility needs to be compensated for is capturing non-cooperative objects such as space debris, where high-bandwidth control is required [1]. The pioneering work by Cannon and Schmitz [2] pertained to the control of flexible-link robots when the sensors and actuators are not co-located. Dwivedy and Eberhard [3] provided an extensive survey of the literature related to the dynamic analysis and control of flexible-joint and flexible-link robots. In general, flexibility can cause steady-state errors, transient errors and vibrations, and even instability in the system. In this paper, we focus on the implications of joint elasticity in the slave robot of a master-slave teleoperation system.

The compliance in the joint of a robot can be modeled by a chained mass-spring-damper system, in which the first mass represents the joint motor whose position is measured and the last mass represents the end-effector by which the robot

makes contact with the environment [4], [5]. In the context of teleoperation control under slave joint compliance, we are interested in control of the slave's end-effector position, which is different from the motor position at least in the transient state, thus position sensing at the end-effector is useful. Depending on the teleoperation architecture and for better performance, we may also need force sensing at the end-effector.

The question that we address in this paper is, what are the performance limitations resulting from joint elasticity in a (rigid-link) slave robot and what added benefits can tip sensors deliver during master-slave teleoperation? Toward this end, we examine the effect of position and force sensors at the tip of an elastic-joint slave on transparency of a teleoperation system. In this initial analysis, a 1-DOF system is considered in order to obtain a fundamental understanding of the implications of joint elasticity during teleoperation. For consistency with the teleoperation literature and without loss of generality, we use velocities rather than positions in models and control laws.

II. Criteria for Analysis of Teleoperation Performance

In an ideal 1-DOF master-slave teleoperation system with hand-master velocity v_h and slave-environment velocity v_e , the dynamics of the master and the slave are

$$f_m + f_h = M_m \dot{v}_h, \quad f_s - f_e = M_s \dot{v}_e \quad (1)$$

where f_h and f_e denote the forces exerted by the operator's hand on the master and by the environment on the slave, respectively. Also, M_m , M_s , f_m and f_s are the master and the slave inertias and control inputs, respectively.

In an *ideally transparent* teleoperation system, regardless of the operator and environment dynamics, we have:

$$v_h = v_e, \quad f_h = f_e \quad (2)$$

Condition (2) guarantees that the dynamics of the environment is displayed to the user with no distortion. With the s -domain hybrid representation of a teleoperation system [6]

$$\begin{bmatrix} F_h(s) \\ -V_e(s) \end{bmatrix} = \begin{bmatrix} h_{11} & h_{12} \\ h_{21} & h_{22} \end{bmatrix} \begin{bmatrix} V_h(s) \\ F_e(s) \end{bmatrix}, \quad (3)$$

(2) can be expressed as

$$H_{\text{ideal}} = \begin{bmatrix} 0 & 1 \\ -1 & 0 \end{bmatrix} \quad (4)$$

Two elements of the H matrix

$$h_{11} = \frac{F_h}{V_h}|_{F_e=0}, \quad h_{21} = -\frac{V_e}{V_h}|_{F_e=0} \quad (5)$$

have direct physical significance. The parameter h_{11} is the impedance transmitted to the user (input impedance) when the slave is in free space. Nonzero values for h_{11} mean that the teleoperation system is providing the user with a "sticky" feel of free-motion movements. The parameter h_{21} is a

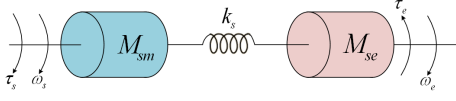


Fig. 1. Schematic diagrams of an elastic-joint manipulator.

measure of velocity tracking fidelity when the slave is in free space. The other two parameters, i.e., $h_{12} = F_h/F_e|_{V_h=0}$ and $h_{22} = -V_e/F_e|_{V_h=0}$ are measures of force tracking fidelity and the output admittance assuming that the master is in contact with an infinitely stiff hand. As discussed in [7], instead of h_{12} and h_{22} , it is more useful to consider elements of the transmission and the impedance matrices

$$f_{12} = \frac{F_h}{F_e}|_{V_e=0}, \quad z_{11} = \frac{F_h}{V_h}|_{V_e=0} \quad (6)$$

The above parameters assume that the slave is in hard contact. The parameter f_{12} shows force tracking fidelity under hard contact ($\rightarrow 1$ ideally) and the parameter z_{11} is the maximum impedance that can be transmitted to the user ($\rightarrow \infty$ ideally), thus quantifying the realism of a user's haptic experience about touching a rigid surface.

Another measure that is dependent on the hybrid parameters but provides important insight into the transparency of a teleoperation system is the environment impedance as transmitted to the user ($\rightarrow Z_e$ ideally)

$$Z_t = \frac{F_h}{V_h} = h_{11} - \frac{h_{12}h_{21}Z_e}{1 + h_{22}Z_e} \quad (7)$$

III. Lumped Model of a 1-DOF Elastic-Joint Slave

The forgoing analysis tools are applicable to general models of the slave robot. We now consider the case when the slave has a flexible coupling between the actuator and the end-effector. Figure 1 shows a rotational two-mass models. An ideal elastic joint can be modeled by a motor with inertia M_{sm} and an end-effector with inertia M_{se} that are coupled via a shaft with a finite stiffness k_s . In this model, τ_s and ω_s are the slave's motor torque and speed, respectively. Also, ω_e is the slave's end-effector (and the environment's) speed and τ_e is the torque applied by the environment on the slave's end-effector.

For compatibility with the common notations in the teleoperation literature, we use the equivalent translational model of the elastic joint in the rest of this paper including in Figure 2, which shows a master-slave system with an elastic-joint slave. The equations of motion of the elastic joint present in Figure 2 are

$$M_{sm}\dot{v}_s = f_s - k_s\Delta x \quad (8)$$

$$M_{se}\dot{v}_e = -f_e + k_s\Delta x \quad (9)$$

$$\Delta x = x_s - x_e \quad (10)$$

where $v_s = \dot{x}_s$ and $v_e = \dot{x}_e$ are the slave's motor and end-effector velocities, respectively. Also, f_s is the force exerted by the slave's actuator on the elastic joint and f_e is exerted by the environment on the slave's end-effector. An s -domain model of this two-input/two-output system is depicted in Figure 3c, in which $Z_{sm} = M_{sm}s$ and $Z_{se} = M_{se}s$.

For simplicity, in this initial analysis, we have not considered backlash or friction in the elastic joint in order to avoid nonlinear terms. Also, we have not considered damping terms in the motor, the end-effector, or the flexible

coupling, but they may easily be factored into the analysis. The master and slave robot actuators are assumed to have unlimited bandwidths compared to the maximum frequency of the desired operating trajectories.

A state-space model of the two-mass system is

$$\begin{aligned} \frac{d}{dt} \begin{pmatrix} v_s \\ \Delta x \\ v_e \end{pmatrix} &= \begin{pmatrix} 0 & -\frac{k_s}{M_{sm}} & 0 \\ 1 & 0 & -1 \\ 0 & \frac{k_s}{M_{se}} & 0 \end{pmatrix} \begin{pmatrix} v_s \\ \Delta x \\ v_e \end{pmatrix} \\ &+ \begin{pmatrix} \frac{1}{M_{sm}} & 0 & 0 \end{pmatrix}^T f_s + \begin{pmatrix} 0 & 0 & \frac{-1}{M_{se}} \end{pmatrix}^T f_e \end{aligned} \quad (11)$$

The above system is state-controllable, meaning that if all states (v_s , Δx and v_e) are measurable, the eigenvalues of the system can be relocated to stable positions via state feedback.

The system (11) has one eigenvalue at the origin of the s -plane and two eigenvalues at $\pm j\omega_R$ where $\omega_R = \sqrt{k_s(1/M_{sm} + 1/M_{se})}$ is the system resonance frequency. For the control input f_s , if v_s is the output, the system will have two zeros at $\pm j\omega_0$ where

$$\omega_0 = \sqrt{\frac{k_s}{M_{se}}} \quad (12)$$

is the system anti-resonance frequency. If v_e is taken as the output, however, the system will show no anti-resonant behavior.

In the context of vibration control of steel rolling mills, which also suffer from flexibility due to the long shafts and gear boxes and have a model similar to (11), it has been shown that the inertia ratio

$$R = \frac{M_{se}}{M_{sm}} \quad (13)$$

plays a key role in shaping the dynamic characteristics of the elastic-joint system. When $R \ll 1$ and there is only feedback of v_s , the system has been reported to show a severely underdamped behavior [8]. In this situation, although the oscillations in v_s may be small, those in v_e may be large. However, with feedback of end-effector velocity v_e , it is possible to dampen such oscillations. In the following section, we examine the effect of joint elasticity in a robot that is acting as the slave during haptic teleoperation.

IV. Possible Teleoperation Architectures vs. Sensor Configurations

We now consider the relationship between the choice of the teleoperation control architecture [9] and the placement of sensors in an elastic-joint slave. Consider the block diagrams in Figure 3, which represent two common teleoperation control architectures. In Figures 3a and b, f_h^* and f_e^* are respectively the operator's and the environment's exogenous input forces and are independent of teleoperation system behavior. We assume that the environment is passive ($f_e^* = 0$) and the operator is passive in the sense that he/she does not perform actions that will make the teleoperation system unstable. In Figures 3a and b, the human operator's hand and the remote environment impedances are denoted by $Z_h(s)$ and $Z_e(s)$, respectively. Also, $C_m = (k_{v_m}s + k_{p_m})/s$ and $C_s = (k_{v_s}s + k_{p_s})/s$ are (PI-type on velocities and PD-type on positions) controllers used locally at the master and the slave, respectively. Lastly, C_1 and C_4 are position gains and C_2 scales the slave/environment interaction as it is fed back to the master.

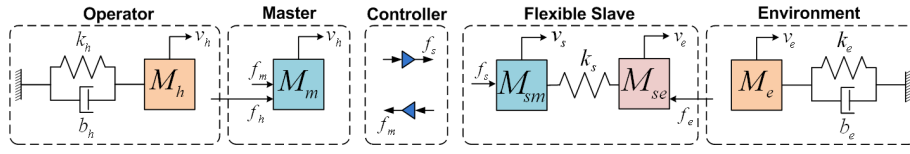


Fig. 2. Models of the operator, master, flexible slave, and environment.

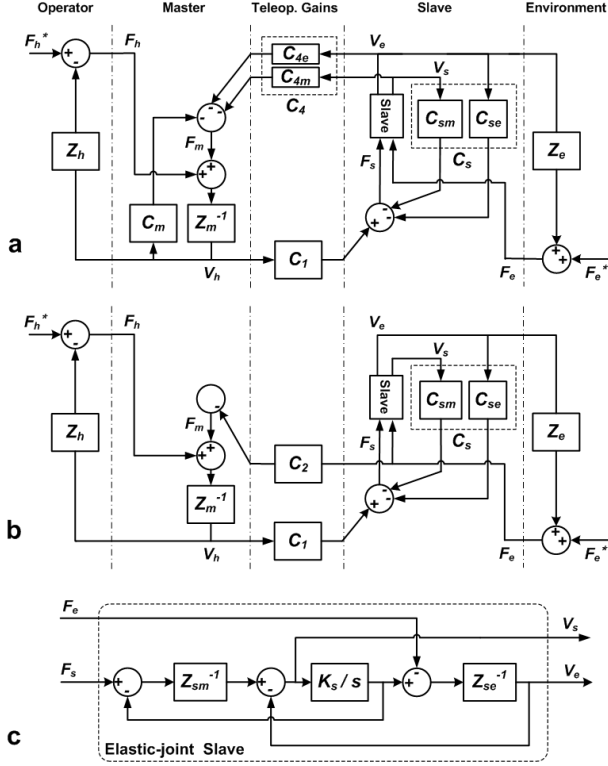


Fig. 3. (a) Position error based (PEB) architecture, (b) direct force reflection (DFR) architecture, and (c) dynamic model of an elastic-joint slave.

In Figures 3a and b, based on (1), the master is shown as the impedance $Z_m^{-1} = 1/(M_m s)$. If the slave has a rigid joint as was assumed in (1), it will be modeled by the impedance $Z_s^{-1} = 1/(M_s s)$. However, for an elastic-joint slave, according to (8)-(10), we have the two-output model shown in Figure 3c. Accordingly, in the presence of joint compliance in the slave, C_s and C_4 are each broken into two separate controllers. As a result, the general control laws for the master and the slave are defined as

$$\begin{aligned} F_m &= -C_m V_h - (C_{4m} V_s + C_{4e} V_e) \quad (\text{Fig. 3a}) \\ F_m &= -C_2 F_e \quad (\text{Fig. 3b}) \\ F_s &= C_1 V_h - (C_{sm} V_s + C_{se} V_e) \quad (\text{Fig. 3a, b}) \end{aligned}$$

A. Teleoperation architectures

For brevity, in the following we use the terms C_s and C_4 , which correspond to a rigid slave. In the presence of joint compliance in the slave, depending on the placement of sensors as discussed in Section IV-B, the above terms are replaced by either C_{sm} or C_{se} and either C_{4m} or C_{4e} .

(1) Position-error based (PEB) control as shown in Figure 3a where $C_1 = C_s$ and $C_4 = -C_m$. Transparency can be improved by selecting $C_1 = Z_s + C_s \doteq Z_{cs}$ and

$$C_4 = -Z_m - C_m \doteq -Z_{cm} \quad (\text{i.e., acceleration feedforward}):$$

$$H = \begin{bmatrix} Z_m + C_m \frac{Z_s}{Z_{cs}} & \frac{C_m}{Z_{cs}} \\ -\frac{C_s}{Z_{cs}} & \frac{1}{Z_{cs}} \end{bmatrix}, \quad H_{\text{acc.}} = \begin{bmatrix} 0 & \frac{Z_{cm}}{Z_{cs}} \\ -1 & \frac{1}{Z_{cs}} \end{bmatrix} \quad (14)$$

For simplicity, in this paper $C_m = C_s$ is chosen.

(2) Direct force reflection (DFR) control as shown in Figure 3b where $C_1 = C_s$ and $C_2 = 1$. Again, transparency is improved by selecting $C_1 = Z_{cs}$:

$$H = \begin{bmatrix} Z_m & \frac{1}{Z_{cs}} \\ -\frac{C_s}{Z_{cs}} & \frac{1}{Z_{cs}} \end{bmatrix}, \quad H_{\text{acc.}} = \begin{bmatrix} Z_m & \frac{1}{Z_{cs}} \\ -1 & \frac{1}{Z_{cs}} \end{bmatrix} \quad (15)$$

B. Sensor configurations

We distinguish four possible sensor configurations for an elastic-joint slave:

- 1) For PEB control, in the simplest case, there is only a velocity sensor on the slave's motor (i.e., v_s feedback).
- 2) For PEB control, an alternative is feedback of v_e using a velocity sensor at the end-effector.
- 3) For DFR control, in the simplest case, there is feedback of v_s and measurement of the end-effector force f_e .
- 4) For DFR control, the other possibility is feedback of v_e and f_e .

Instead of using sensors to measure the end-effector velocity v_e and the external force f_e , these quantities may be estimated using an extended state observer [10]. In the following section, we examine the effect of joint elasticity in a robot that is acting as the slave during haptic teleoperation.

V. Effect of Joint Elasticity on Transparency

A. PEB control based on feedback of v_s

With no feedback of v_e , we have $C_{se} = C_{4e} = 0$ in Figure 3a. The PEB control with feedback of v_s is designed as follows. We choose identical local PI controllers $C_m = C_{sm} = k_p + k_i/s$, and $C_{4m} = -Z_m - C_m$. Since the elastic-joint slave is comprised of two inertias, we consider the general term $C_1 = \eta_1 Z_{sm} + \eta_2 Z_{se} + C_{sm}$ where η_1 and η_2 are non-negative constants. As a result, the parameter h_{21} involves terms such as $k_i + k_p s + \eta_1 M_{sm} s^2 + \eta_2 M_{se} s^2$ in both its numerator and denominator, motivating the selection of $\eta_1 = 1$, $\eta_2 = 0$, $k_i = \beta^2 M_{sm}$ and $k_p = 2\beta M_{sm}$ (for critical damping) where $\beta > 0$ is a control gain affecting the placement of poles in the system.

The resulting four measures of transparency defined in Section II are

$$h_{11} = M_{se} s \frac{1 + (R' - 1) \left(\frac{s}{s+\beta} \right)^2}{1 + \left(\frac{s}{\omega_0} \right)^2 + R s^2 \left(\frac{s}{s+\beta} \right)^2} \quad (16)$$

$$h_{21} = \frac{-1}{1 + \left(\frac{s}{\omega_0} \right)^2 + R \left(\frac{s}{s+\beta} \right)^2} \quad (17)$$

$$\frac{1}{f_{12}} = \frac{1}{1 + (R' - 1) \left(\frac{s}{s+\beta} \right)^2} \quad (18)$$

$$z_{11} = M_{se} s \frac{1 + (R' - 1) \left(\frac{s}{s+\beta} \right)^2}{\left(\frac{s}{\omega_0} \right)^2 + R \left(\frac{s}{s+\beta} \right)^2} \quad (19)$$

where

$$R' = \frac{M_m}{M_{sm}} \quad (20)$$

and ω_0 and R have been defined in (12) and (13), respectively. The reason for using $1/f_{12}$ is to have a proper transfer function as in the presence of flexibility the order of the numerator of f_{12} increases. It can be seen that if $k_s \rightarrow \infty$ and $R \rightarrow 0$, the parameters corresponding to the rigid case (e.g., h_{11} and h_{21} of H_{acc} . in (14)) will be retrieved.

Assuming the PI controller $C_m = C_{sm}$ does not become saturated, the control parameter β can be selected to be sufficiently large so that the dynamics contributed by the controller (i.e., involving $(s + \beta)^2$) is much faster than the one originating from the rest of the system including joint flexibility. With this assumption, we get the simplified performance indices listed in the first column of Table I.

While the above four parameters only depend on the teleoperation system, the impedance transmitted to the user is also a function of the environment impedance Z_e . Assuming a linear spring model $Z_e = k_e/s$ for the environment (i.e., $M_e = 0$ and $b_e = 0$ in Figure 2),

$$Z_t = \frac{1/s}{\frac{1}{k_s} + \frac{1/k_e}{1+M_{se}/k_e s^2}} \quad (21)$$

The transmitted impedance represents the combined effect of h_{11} and z_{11} . Evidently, when the slave is in free space ($k_e \rightarrow 0$), we will have $Z_t \rightarrow h_{11}$, and when it is in contact with a hard environment ($k_e \rightarrow \infty$), then $Z_t \rightarrow z_{11}$.

B. PEB control based on feedback of v_e

With feedback of v_e , we have $C_{sm} = C_{Am} = 0$ in Figure 3a. Again, $C_m = C_{se} = k_p + k_i/s$, $C_{4e} = -Z_m - C_m$, and $C_1 = \eta_1 Z_{sm} + \eta_2 Z_{se} + C_{se}$. For reasons similar to the case with feedback of v_s , we choose $\eta_1 = 1$, $\eta_2 = 0$, $k_i = \beta^2 M_{sm}$ and $k_p = 2\beta M_{sm}$. The transparency indices for PEB control with feedback of v_e when β is sufficiently large are listed in Table I.

C. DFR control based on feedback of v_s and f_e

With feedback of v_s , we have $C_{se} = 0$ in Figure 3b. Also with DFR control, $C_2 = 1$ and $C_{sm} = k_p + k_i/s$. With C_1 chosen as in PEB control, the simplified transparency indices for large β are listed in Table I.

D. DFR control based on feedback of v_e and f_e

With feedback of v_e , we have $C_{sm} = 0$ in Figure 3b. Also, $C_2 = 1$ and $C_{se} = k_p + k_i/s$. With C_1 chosen as in PEB control, the corresponding transparency indices for large β are listed in Table I.

VI. Simulation Study

In order to confirm the transparency results of Table I, we simulated the PEB and DFR teleoperation control architectures in SimuLink using a variable-step, continuous-time ode23 solver. We chose $M_m = M_{sm} = 1$ kg, $M_{se} = 0.1$ kg, $k_s = 1000$ N/m, and therefore $R = 0.1$, $R' = 1$ and $\omega_0 = 100$ rad/sec. Also, the control parameter $\beta = 10^6$ was chosen to be large as was assumed in Table I. The excitation input f_h in Figure 2 consisted of the sum of a number of sinusoids evenly-spaced in the frequency domain from zero to 1000 rad/sec. The reason for this choice is that a multi-sine signal demonstrates a rich and almost uniform spectrum over the frequency range of interest and is highly persistent

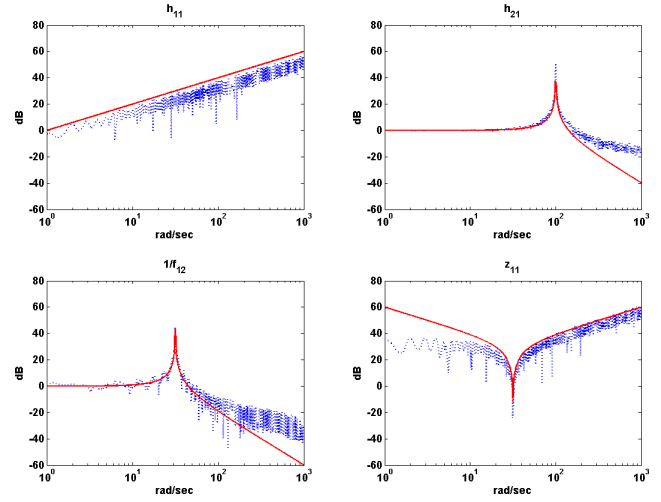


Fig. 4. Magnitudes of the performance indices for DFR teleoperation with feedback of v_s and f_e when $R = 0.1$, $R' = 1$ and $\omega_0 = 100$ rad/sec. Simulation results (dashed) and idealized models (solid).

excitation (pe) as the sum of n sinusoids is pe of an order not less than $2n - 2$. Free-motion and hard-contact tests were simulated for 20 seconds using $k_e = 0$ and $k_e = 10^7$ N/m, respectively. By applying spectral analysis (MATLAB function spa), h_{11} and h_{21} were estimated using the free-motion test data via (5), and $1/f_{12}$ and z_{11} were estimated using the hard-contact test data via (6). As an example, the estimated magnitudes of the performance indices for DFR teleoperation with feedback of v_s and f_e are shown in Figure 4 (dashed lines), which closely follow the idealized indices listed in the third column of Table I (solid lines).

VII. Discussion

The results of the above analysis as listed in Table I are useful for understanding how extra sensors at the end-effector (tip) of an elastic-joint slave robot can enhance transparency. With minimally invasive surgical robots as one of the candidates for which such an analysis is justified, however, arguments against adding sensors at the robot tip are made based on the fact that such sensors can complicate the design of the robotic arm, create sterilization issues, and ultimately raise the cost of the system. As a result, tip sensors have so far been avoided in today's commercial surgical systems (e.g., the da Vinci system from Intuitive Surgical Inc., Sunnyvale, CA). On the other hand, in the specific example of the da Vinci robot, in order to avoid joint compliance, tensions in the cable drives are high. This has resulted in large friction in the instruments' drive trains, requiring sizable, remotely-based motors for tip actuation. In general, however, given the trade-off between joint compliance and friction in cable drives, joint compliance should be addressed separately especially in robots that are designed to be lightweight and cannot accommodate large actuators. Therefore, the question addressed in this paper is, regardless of the state of sensor/actuator technologies in terms of meeting the requirements for integration in surgical or space robots, what added benefits in terms of teleoperation transparency can tip sensors deliver during teleoperation with a compliant-joint slave?

The transparency indices listed in Table I are idealized to ignore the effect of controller dynamics by assuming $\beta \rightarrow \infty$, which corresponds to perfect local position control of the slave (and the master during PEB control). This is

TABLE I

PERFORMANCE INDICES OF DIFFERENT TELEOPERATION ARCHITECTURES AND SENSOR CONFIGURATIONS ASSUMING NO ACTUATOR SATURATION.

Teleoperation architecture	PEB	PEB	DFR	DFR	Ideal
Sensor measurements	v_s	v_e	v_s and f_e	v_e and f_e	value
h_{11} (free-motion transmitted impedance)	$\frac{M_{se}s}{1+(\frac{s}{\omega_0})^2}$	$M_{se}s + M_{sm}^2s(\frac{s}{\omega_0})^2$	M_ms	M_ms	0
h_{21} (free-motion position tracking)	$\frac{-1}{1+(\frac{s}{\omega_0})^2}$	-1	$\frac{-1}{1+(\frac{s}{\omega_0})^2}$	-1	-1
$\frac{1}{f_{12}}$ (hard-contact force tracking)	1	$1 + \frac{1}{R}(\frac{s}{\omega_0})^2$	$\frac{1}{1 + \frac{R'}{R}(\frac{s}{\omega_0})^2}$	1	1
z_{11} (hard-contact transmitted impedance)	$\frac{k_s}{s}$	∞	$M_ms + \frac{k_s}{s}$	∞	∞

a simplification that is made to isolate the effect of joint elasticity. With this assumption, Section VII-A is aimed at understanding the fundamental limitations imposed by joint elasticity on teleoperation transparency and the added benefits of using extra sensors at the output shaft of the elastic joint. In practice, however, β cannot be infinitely large, thus bringing in the controller dynamics and limiting the performance. In Section VII-B, we investigate the effect of limited control action on transparency, specifically the indices for motion tracking and force tracking.

A. Case of no actuator saturation

Based on Table I, which assumes β is very large, the following conclusions can be made:

- From the first row (h_{11}), while during PEB teleoperation the user will feel some residual impedance that depends on the slave's mass and stiffness characteristics, during DFR teleoperation only the master inertia will be transmitted to the user. If acceleration feedforward is not provided during PEB, the user will feel the master inertia as well.
- From the second row (h_{21}), with feedback of v_e , perfect position tracking can be attained in both PEB and DFR teleoperation regardless of the joint compliance. With feedback of v_s , however, position tracking is satisfactory only in low frequencies.
- From the third row ($1/f_{12}$), perfect force tracking can be attained in PEB teleoperation with feedback of v_s and in DFR teleoperation with feedback of v_e . Otherwise, force tracking is satisfactory only in low frequencies.
- From the fourth row (z_{11}), without knowledge of v_e , the elasticity in the joint will be felt by the user during a hard contact task. With feedback of v_e , however, hard surfaces can be displayed transparently to the user in both PEB and DFR teleoperation.

B. Effect of avoiding actuator saturation on transparency

Table I is accurate only for $\beta \rightarrow \infty$, yet the relative performance of different teleoperation architectures and sensor configurations can be inferred from it for the case that β is limited. Here we focus on the effect of β on motion tracking and force tracking. It was shown that with feedback of v_e and $\beta \rightarrow \infty$, it is possible to achieve ideal free-motion position tracking ($h_{21} = -1$) regardless of the joint compliance. This is not possible with feedback of v_s even when $\beta \rightarrow \infty$. Also, ideal hard-contact force tracking ($1/f_{12} = 1$) is possible with feedback of v_e in DFR teleoperation, which is not attainable with feedback of v_s . In the following we examine the effect of β on h_{21} and $1/f_{12}$ for these two possible sensor configurations.

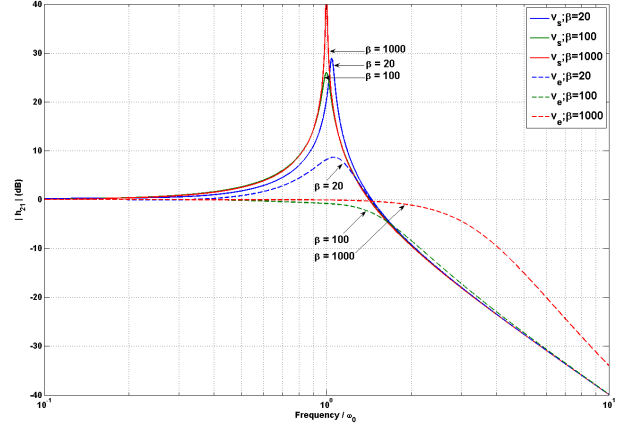


Fig. 5. Magnitude of h_{21} with feedback of v_s (solid lines) and feedback of v_e (dashed lines) vs. normalized frequency when $R = 0.1$.

1) Free-motion position tracking

For teleoperation with feedback of v_s , h_{21} (for both PEB and DFR) is given by

$$h_{21}|_{v_s} = \frac{-1}{1 + (\frac{s}{\omega_0})^2 + R(\frac{s}{s+\beta})^2} \quad (22)$$

For teleoperation with feedback of v_e , the parameter h_{21} (for both PEB and DFR) is given as

$$h_{21}|_{v_e} = \frac{-1}{1 + \left(R + (\frac{s}{\omega_0})^2\right) \left(\frac{s}{s+\beta}\right)^2} \quad (23)$$

The magnitudes of the above two responses are plotted in Figure 5 when $\omega_0 = 100$ rad/sec, $R = 0.1$ and $\beta = 20, 100, 1000$. As can be seen, for v_s feedback, $h_{21}|_{v_s} \approx 1$ only for frequencies lower than ω_0 regardless of β . However, for v_e feedback, we can increase the maximum frequency below which $h_{21}|_{v_e} \approx 1$ by increasing β . Therefore, the frequency range of position tracking is improved if feedback of v_e is provided and high-gain controllers are used. This is consistent with the discussion in Section III that the two-mass system (11) has an anti-resonance at ω_0 if v_s is the output but has no anti-resonance if v_e is the output. Therefore, the presence of a velocity (or position) sensor at the output shaft of the elastic joint facilitates high-bandwidth position tracking during both PEB and DFR teleoperation.

To further investigate the effect of β and R on the shape of h_{21} , in Figure 6 the cutoff frequency ω_c (the frequency at which the magnitude drops by -3 dB compared to low frequencies) of h_{21} is plotted versus β for $\omega_0 = 100$ rad/sec, $R = 0.1, 1, 10$ and for feedback of v_s (solid lines) and feedback of v_e (dashed lines). As can be seen, with feedback of v_s , as $\beta \rightarrow \infty$ the cutoff frequency of h_{21} given by (22)

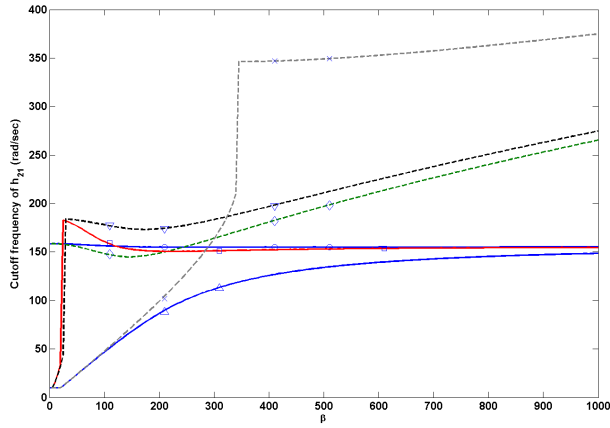


Fig. 6. Cutoff frequency of h_{21} with feedback of v_s (solid lines) and feedback of v_e (dashed lines) when $\omega_0 = 100$ rad/sec. \circ : feedback of v_s and $R = 0.1$; \diamond : feedback of v_e and $R = 0.1$; \square : feedback of v_s and $R = 1.0$; ∇ : feedback of v_e and $R = 1.0$; \triangle : feedback of v_s and $R = 10$; \times : feedback of v_e and $R = 10$.

approaches $(\sqrt{2} + 1)^{1/2}\omega_0 = 155$ rad/sec. In contrast, with feedback of v_e , the cutoff frequency of h_{21} given by (23) continues to grow as β increases, thus ensuring good position tracking over a wider frequency range. The other conclusion from Figure 6 is that when R is not small and β is not large (i.e. M_{se} is comparable with or larger than M_{sm} and the control effort applied on M_{sm} is limited), the position tracking bandwidth is severely limited even with feedback of v_e as the cutoff frequency of h_{21} drops below ω_0 . Therefore, as R gets larger, the demand for higher control actions (higher β) increases to attain satisfactory position tracking.

2) Hard-contact force tracking

In DFR teleoperation, $1/f_{12}$ for the two different position feedback possibilities is given by

$$\frac{1}{f_{12}} \Big|_{\text{DFR}, v_s} = \frac{1}{1 + \frac{R'}{R} \left(\frac{s}{\omega_0}\right)^2 + R' \left(\frac{s}{s+\beta}\right)^2} \quad (24)$$

$$\frac{1}{f_{12}} \Big|_{\text{DFR}, v_e} = \frac{1}{1 + \frac{R'}{R} \left(\frac{s}{\omega_0}\right)^2 \left(\frac{s}{s+\beta}\right)^2 + R' \left(\frac{s}{s+\beta}\right)^2} \quad (25)$$

Somewhat similar to the case with h_{21} , when we have feedback of v_s , near-ideal force tracking under hard-contact is obtained only for frequencies lower than $\omega_0\sqrt{R/R'}$ regardless of the maximum control effort. In contrast, with v_e , the cutoff frequency of $1/f_{12}$ can be increased by increasing β . Therefore, in DFR teleoperation, feedback of v_e also helps to achieve high-bandwidth force tracking. The magnitudes of $1/f_{12}$ and the relationship between the cutoff frequency of $1/f_{12}$ and β are similar to those in Figures 5 and 6 for h_{21} , and are not shown here.

VIII. Concluding Remarks

This paper analyzed the limitations imposed by the slave robot joint compliance on teleoperation transparency and evaluated the added benefits of using extra sensors at the end-effector (tip) of the elastic-joint slave robot. It was shown that for both position error based and direct force reflection teleoperation architectures, velocity (or position) feedback from the end-effector of the elastic-joint slave improves free-space position tracking performance, which is otherwise hampered by the joint's anti-resonance. Also, in direct force reflection teleoperation, the tip velocity feedback improves hard-

contact force tracking performance. Over low frequencies, free-space position tracking and hard-contact force tracking are both satisfactory even in the absence of tip velocity feedback, however in terms of the transmitted impedance it was shown that the only way to eliminate the display of joint elasticity to the user during a hard contact task is to use tip velocity feedback in either teleoperation architecture.

The investigation of the effect of joint elasticity on teleoperation stability remains as future work. Our preliminary results show that absolute stability (stability under all passive terminations $Z_h(s)$ and $Z_e(s)$) is guaranteed either unconditionally or below certain frequencies depending on the teleoperation architecture and sensor configuration. Nonetheless, the very presence of an environment (and an operator) provides negative feedback and has a stabilizing effect, thus increasing the frequency range of stable operation.

Flexibility in the links of a slave robot has similar and potentially more severe implications in terms of the transparency and stability of teleoperation. Surgical robots are a typical example of flexible-link slave teleoperation systems as laparoscopic instruments are slim and deflect significantly [11]. In future, we will try to perform a similar analysis on the effect of link flexibility during bilateral teleoperation and explore ways to minimize it.

Acknowledgements

This research was supported by the National Science Foundation grant EEC-9731748 and a postdoctoral fellowship awarded to the first author by the Natural Sciences and Engineering Research Council of Canada. The authors acknowledge the helpful discussions with Allison M. Okamura and Katherine J. Kuchenbecker at Johns Hopkins Laboratory for Haptic Exploration.

References

- [1] S. Nishida and T. Yoshikawa, "Space debris capture by a joint compliance controlled robot," in *Proceedings of IEEE/ASME International Conference on Advanced Intelligent Mechatronics*, vol. 1, Kobe, Japan, July 2003, pp. 496–502.
- [2] R. H. Cannon and E. Schmitz, "Initial experiments on the end-point control of a flexible one-link robot," *The International Journal of Robotics Research*, vol. 3, no. 3, pp. 62–75, 1984.
- [3] S. K. Dwivedy and P. Eberhard, "Dynamic analysis of flexible manipulators, a literature review," *Mechanism and Machine Theory*, vol. 41, no. 7, pp. 749–777, July 2006.
- [4] M. W. Spong, "Modeling and control of elastic joint robots," *ASME Journal of Dynamic Systems, Measurement and Control*, vol. 109, no. 4, pp. 310–319, 1987.
- [5] J. K. Mills, "Stability and control of elastic-joint robotic manipulators during constrained-motion tasks," *IEEE Transactions on Robotics*, vol. 8, no. 1, pp. 119–126, February 1992.
- [6] B. Hannaford, "A design framework for teleoperators with kinesthetic feedback," *IEEE Transactions on Robotics and Automation*, vol. 5, pp. 426–434, 1989.
- [7] I. Aliaga, A. Rubio, and E. Sanchez, "Experimental quantitative comparison of different control architectures for masterslave teleoperation," *IEEE Transactions on Control Systems Technology*, vol. 12, no. 1, pp. 2–11, January 2004.
- [8] G. Zhang and J. Furusho, "Speed control of two-inertia system by PI/PID control," *IEEE Transactions on Industrial Electronics*, vol. 47, no. 3, pp. 603–609, June 2000.
- [9] M. Tavakoli, A. Aziminejad, R. V. Patel, and M. Moallem, "Enhanced transparency in haptics-based master-slave systems," in *Proceedings of American Control Conference*, New York, NY, July 2007, pp. 1455–1460.
- [10] R. Zhang and C. Tong, "Torsional vibration control of the main drive system of a rolling mill based on an extended state observer and linear quadratic control," *Journal of Vibration and Control*, vol. 12, no. 3, pp. 313–327, 2006.
- [11] R. A. Beasley and R. D. Howe, "Model-based error correction for flexible robotic surgical instruments," in *Proceedings of Robotics: Science and Systems Conference*, Cambridge, MA, June 2005, pp. 359–364.